Physica B 581 (2020) 411953

Contents lists available at ScienceDirect

Physica B: Physics of Condensed Matter

journal homepage: http://www.elsevier.com/locate/physb

Investigation of enhanced far-red emitting phosphor $GdAlO_3:Mn^{4+}$ by impurity doping for indoor plant growth LEDs

Xin Li [a], Wenhao Li [b,**], Bofei Hou [a], Mochen Jia [a], Yang Xu [a], Mingxuan Zhang [a], Huayao Wang [a], Zuoling Fu [a,*]

[a] Coherent Light and Atomic and Molecular Spectroscopy Laboratory, Key Laboratory of Physics and Technology for Advanced Batteries, College of Physics, Jilin University, Changchun, 130012, China

[b] Changchun Institute of Optics, Fine Mechanics and Physics, Chinese Academy of Sciences, Changchun, Jilin, 130033, China

ARTICLE INFO

Keywords:
Mn^{4+} luminescence
Indoor plant growth LEDs
Far-red-emitting
Phytochrome P_{FR}

ABSTRACT

Phytochrome is indispensable for plant growth, which can absorb light useful for sprout, blossom, fruits. Generally, Phytochrome P_R absorbs red light and Phytochrome P_{FR} absorbs far-red light. The emission of Mn^{4+} doped $GdAlO_3$ is situated in far-red light region. Herein, $GdAlO_3:Mn^{4+}$, Mg^{2+}($GAL:Mn^{4+}$, Mg^{2+}) phosphors were successfully synthesized via sol-gel method and the crystalline structure and luminescence properties were investigated systematically. Impressively, the emission intensity of GAL: Mn^{4+} phosphors was raised by Mg^{2+} and Ge^{4+} doping, and the mechanism of improved luminescence was also discussed. Depending on photoluminescence excitation and photoluminescence spectroscopy, the crystal field strength of the $GdAlO_3$ host was calculated. In addition, excellent color purity and good thermal stability were found in Mg^{2+} co-doped $GdAlO_3:Mn^{4+}$ phosphors. Furthermore, the luminescence spectrum of GAL: Mn^{4+}, Mg^{2+} phosphor was agreed well with the absorption of Phytochrome P_{FR}, which convincingly confirmed that Mg^{2+} co-doped $GdAlO_3:Mn^{4+}$ phosphors show promise in indoor plant growth LEDs.

1. Introduction

Cultivating plants indoors, as a remarkably popular method, is attracting gigantic attention due to its relatively stable environment and the ability to resist the changeable climate including droughts, storms, waterfloods and insect pests [1–3]. Light is a critical requirement for the growth of plants indoors, which is pivotal energy for the photosynthesis and can also provide the energy for sprout, blossom, fruits and other morphogenesis of plants. In addition, some previous investigations have demonstrated that light of various wavelength spectra have different influences on plants growth. For instance, blue light (400–500 nm), red (620–690 nm) and far red (700–740 nm) light are vital for photosynthesis, phototropism, and photomorphogenesis, respectively [4,5]. Nowadays, the illuminants applied in cultivating plants indoors are usually traditional categories, such as incandescent lamps, fluorescent lamps and high-pressure sodium lamps [6]. Apparently, the traditional lamps for cultivating plants indoors have some severe disadvantages, such as high energy consumption, the mismatches between their emitting spectra and the absorption spectra of plants [7]. LEDs based solid-state light technology can effectively avoid abovementioned shortcomings of traditional light sources, because LEDs have beneficial merits, such as energy saving, long lifetime, low heat generating and environmental friendliness [8,9]. Moreover, choosing suitable materials and appropriate chips can lead to produce the most exceptional spectra of plants growth. Phosphor-converted LEDs were fabricated by combining the InGaN or GaN chip and the packaging materials including phosphors and encapsulants to obtain the final devices, which is a prospective artificial illuminants applied in agriculture and horticulture indoors [10,11]. The phosphors play an important role in fabricating LED devices, which can affect the luminous efficiency, lifetime and spectral composition [12,13]. Herein, against this background, it is a vital matter to develop the high quality phosphors which have wide scope red and far-red emitting and strong absorption in blue light and near ultraviolet light region for cultivating plants indoors.

There are a variety of blue-emitting and red-emitting materials suitable for indoor plant growth LEDs in scientific research field which

* Corresponding author.
** Corresponding author.
E-mail addresses: liwh@ciomp.ac.cn (W. Li), zlfu@jlu.edu.cn (Z. Fu).

https://doi.org/10.1016/j.physb.2019.411953
Received 11 September 2019; Received in revised form 5 December 2019; Accepted 14 December 2019
Available online 16 December 2019

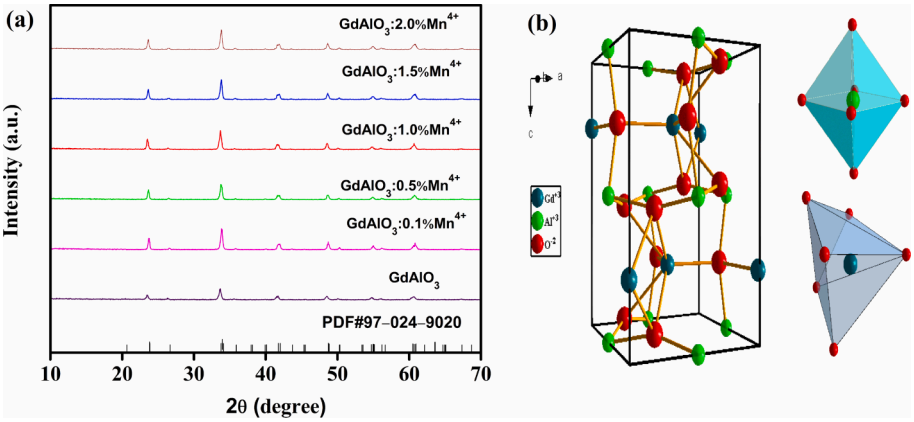

Fig. 1. (a) XRD pattern of $GdAlO_3$: xMn^{4+}; (b) Crystal structure of $GdAlO_3$.

have been reported. Deng et al. covered that red-emitting $3.5MgO{\cdot}0.5MgF_2{\cdot}GeO_2{:}Mn^{4+}$ combinating 420 nm blue chip fabricated LEDs were used to cultivate milk-Chinese cabbage and made a good result [14]. Tamulaitis et al. reported that AlGaInP LED cultivated radish and lettuce [15]. Moreover, some far-red emitting phosphors synthesized via solid-state synthesis route applied for LEDs for plants growth also have been investigated so far [16–18]. However, the synthesis of far-red emitting materials by sol-gel method is rare, which can effectively avoid ultrahigh calcination temperature. In this work, Mn^{4+} doped $GdAlO_3$ farred emitting novel phosphors were prepared by a sol-gel method. The crystal structure, luminescence properties and concentration-related emission of non-rare earth phosphor were investigated and analyzed. In addition, we also probed into the luminescence behaviors of Mn^{4+} in $GdAlO_3$ substrate via different impurity ions co-doping and explained the relevant mechanism. The crystal field strength parameters Dq, Racah parameter B and C of the $GdAlO_3$ host were evaluated and temperature-related emission spectra of $GdAlO_3$:5% Mn^{4+}, 2%Mg^{2+} (abbreviated as: GAL:Mn^{4+}, Mg^{2+}) phosphor were discussed. Good thermal stability, high color purity and coinciding well with Phytochrome P_{FR} vigorously demonstrated that Mg^{2+} co-doped GAL: Mn^{4+} phosphor has an anticipated capacity for indoors plant growth LEDs.

2. Experimental section

2.1. Raw materials

The starting raw materials of $Gd(NO_3)_3{\cdot}6H_2O$ (99.99%), $Al(NO_3)_3{\cdot}9H_2O$ (99.99%), $Mn(NO_3)_2{\cdot}4H_2O$ (98%), MgO (99.99%), GeO_2 (99.99%), $LiNO_3$(99.99%), citric acid were purchased from Aladdin and used without further purified. $Mg(NO_3)_2$ and $Ge(NO_3)_4$ were obtained by MgO and GeO_2 reaction with nitrate solution.

2.2. Sample preparation

A series of Mn^{4+} doped $GdAlO_3$ phosphors were synthesized by sol-gel method. Based on the formula of Mn^{4+}/A (x/y): $GdAl_{1-x-y}O_3$, wherein x stands for the amount of Mn^{4+}, and y represents the amount of the co-doping cation A, corresponding nitrate solution was mixed and the citric acid was added to the metal ions solution as the chelating agent. The stoichiometric proportion of citric acid to total metal-ions was 2: 1. The mixture was stirring for some time to form the extremely transparent solution. Then, the transparent solution was dried at 90 °C for 24 h to obtain the light brown gels. After calcination at 500 °C for 2 h, the precursors were obtained. Eventually, the precursors were further sintered at 1000 °C for 4 h and thoroughly grounded for 30 min.

2.3. Characterization

The powder XRD data for phase identification were recorded with on

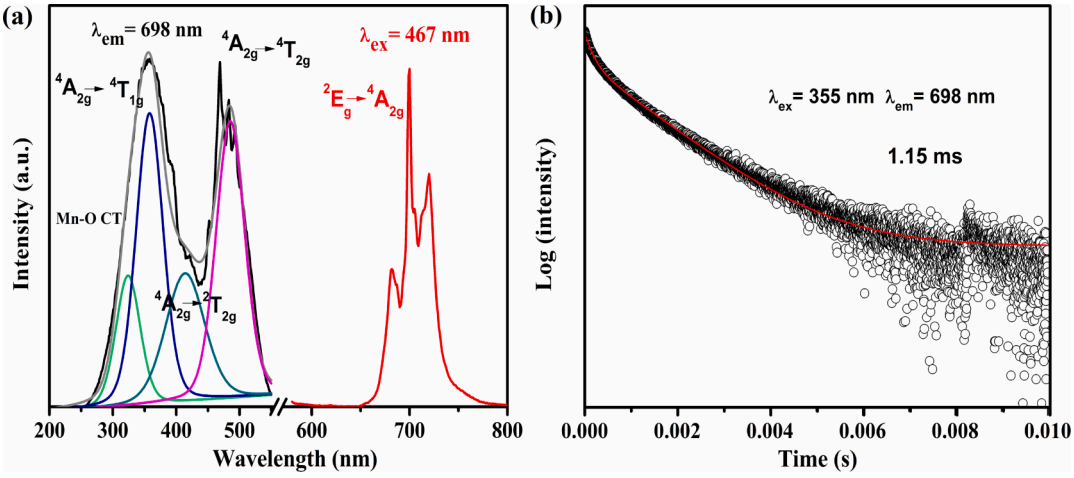

Fig. 2. (a) PLE spectra (λ_{em} = 698 nm) and PL spectra (λ_{ex} = 467 nm) of $GdAlO_3$:0.5%Mn^{4+}; (b) Decay curve of Mn^{4+} ^2E_g excited state in $GdAlO_3$: 0.5%Mn^{4+} under 355 nm UV light excitation.

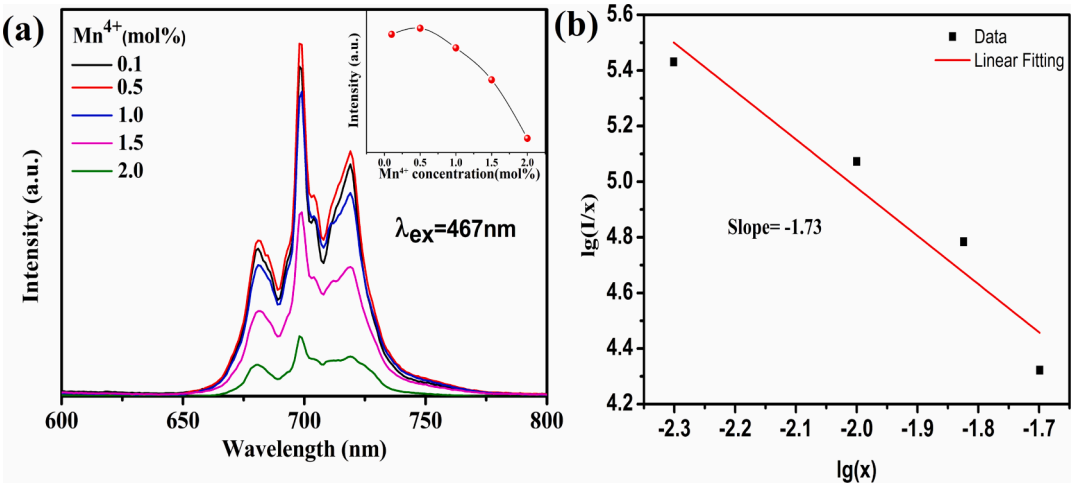

Fig. 3. (a) The PL spectra of $GdAlO_3$:xMn^{4+}(x = 0.1–2.0%) phosphors excited at 467 nm; (b) The relationship between log (I/x) and log(x) of $GdAlO_3$:Mn^{4+}(x represents the concentration of Mn^{4+}).

a Rigaku-Dmax 2500 diffractometer in the 2θ range from 10° to 80° using Cu Kα radiation (λ = 0.15405 nm). Excitation and emission spectra were recorded on a Zolix spectrofluorometer with a LSP-150 W Xe lamp. The phosphors were located in a copper tank with the increasing temperature heated by resistive wire elements to get temperature-related spectra. The measurements of PL decay lifetime were implemented using a time-correlated single-photon counting (TCSPC) lifetime spectroscopy system with a 355 nm laser source. Absolute photoluminescence quantum yields (QYs) were measured by the absolute PL quantum yield measurement system (C9920–02, Hamamatsu Photonics K. K., Japan).

3. Results and discussion

3.1. Phase formation and crystal structure

The XRD patterns of $GdAl_{1-x}O_3$: xMn^{4+} (x = 0, 0.1%, 0.5%, 1%, 1.5%, 2%) (GAL: Mn^{4+}) phosphors are demonstrated in Fig. 1(a). As shown in Fig. 1(a), the synthesized samples show a pure $GdAlO_3$ phase, well indexed to PDF#97-024-9020, indicating that no impurity phases are introduced with the addition of Mn^{4+}. The crystal structure of the $GdAlO_3$ orthorhombic phase is judged with lattice parameters of a = 5.2537 Å, b = 5.3039 Å, c = 7.4435 Å and a space group of Pnma [19]. Corresponding crystal structure of $GdAlO_3$ is established by applying Diamond software and unit cell structures of pure $GdAlO_3$ are shown in Fig. 1(b). As illustrated in Fig. 1(b), Gd atoms are coordinated to six O atoms and Al atoms are coordinated to six O atoms presenting the octahedron structure in the $GdAlO_3$ crystal. In $GdAlO_3$: Mn^{4+} phosphors, the ion radius of Mn^{4+} (r = 0.053 nm) is closer to the ionic of Al^{3+}(r = 0.0535 nm). Thus, Mn^{4+} ions easily occupy Al^{3+} ions sites in the $GdAlO_3$ host [20].

3.2. Luminescence behaviors

The photoluminescence excitation (PLE) (λ_{em} = 698 nm) and photoluminescence spectroscopy (PL) (λ_{ex} = 467 nm) spectra were recorded at room temperature to explore the photoluminescence properities of GAL:Mn^{4+} and are presented in Fig. 2(a). The PLE spectrum monitored at 698 nm consists of two broad bands, which can be fitted by four Gaussian curves with the center peak value at 321, 360, 416 and 483 nm, are attributed to Mn–O charge-transfer band, ground state $^4A_{2g}$ to excitation states $^4T_{1g}$, $^2T_{2g}$, $^4T_{2g}$, respectively [21,22]. It is worth nothing that GAL:Mn^{4+} can be excited by 360 nm and that means the phosphor can be availably excited by near UV, UV and blue LED chips for its application. As demonstrated in PL, we can judge the Mn^{4+} in weak or strong crystal cases preliminarily. Generally, in the weak crystal field cases, the emission spectrum consists of $^4T_2$ -$^4A_2$ spin allowed transition, which displays a broad band. However, in the strong crystal field, the emission spectra appear as a sharp peak originating from ^2E-$^4A_2$ spin forbidden transition [23]. Therefore, we can judge the Mn^{4+} in strong crystal cases preliminarily. In addition, As shown in Fig. 2(a), in the emission spectrum of Mn^{4+} doped $GdAlO_3$, it includes three peaks at 682 nm, 698 nm and 720 nm owning to different lattice vibrations of Mn^{4+} ion in octahedral symmetry [24,25].

Fig. 2(b) demonstrates the luminescence decay curve of the GAL:0.5% Mn^{4+} sample. The decay lifetime of the sample is fitted with double exponential expression[12,26].

$$I = A_1 \exp(-t/\tau_1) + A_2 \exp(-t/\tau_2) \quad (1)$$

where I is the luminescent emission intensity of the GAL:0.5%Mn^{4+} sample, τ_1 and τ_2 are the lifetime components, A_1 and A_2 are constants. The average lifetime can be obtained according to the following expression:

$$\tau = \frac{A_1\tau_1^2 + A_2\tau_2^2}{A_1\tau_1 + A_2\tau_2} \quad (2)$$

The fitting results of τ_1, τ_2 and A_1, A_2 are 0.000170 s, 0.00128 s and 211.05, 220.50, respectively. The decay lifetime of the GAL:0.5%Mn^{4+} is 1.15 ms according to equation (2) via fitting and calculating. The bi-exponential fitting is also presented in Mn^{4+} doped $CaYAlO_4$ phosphors [22]. In $GdAlO_3$ structure, Al has only one site and Mn^{4+} substituted the Al^{3+} site. We considered that the phenomenon was ascribed to the defect-induced non-radiative transition, which was originated from the charge mismatch between Mn^{4+} and Al^{3+} [27].

Fig. 3(a) displays PL spectra of $GdAlO_3$:xMn^{4+}excited at 467 nm (x = 0.1%, 0.5%, 1%, 1.5%, 2%). The position and shape of samples with different Mn^{4+} contents are identical except the relative intensity. The luminescence intensity increases gradually with increasing of Mn^{4+}concentrations. From the inset of Fig. 3(a), when the Mn^{4+} concentration x reaches 0.5%, the luminescence intensity reaches maximum, then decreases with further increase of Mn^{4+} concentrations, which is attributed to concentration quenching effect [28]. Generally speaking, concentration quenching often happens in rare-earth or transition metal ions doped phosphors owning to the energy transfer between neighboring cations. The critical distance (R_c) is an important parameter in quenching mechanism which can be calculated using the following formula [29,30].

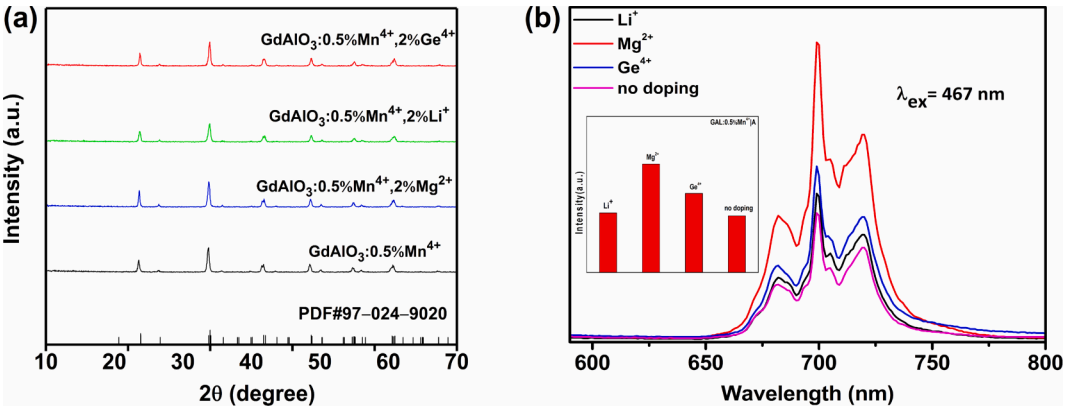

Fig. 4. (a) XRD pattern of different ions co-doped $GdAlO_3$:0.5%Mn^{4+}; (b) The emission spectra of $GdAlO_3$:0.5%Mn^{4+} with different impurity doping under the excitation of 467 nm.

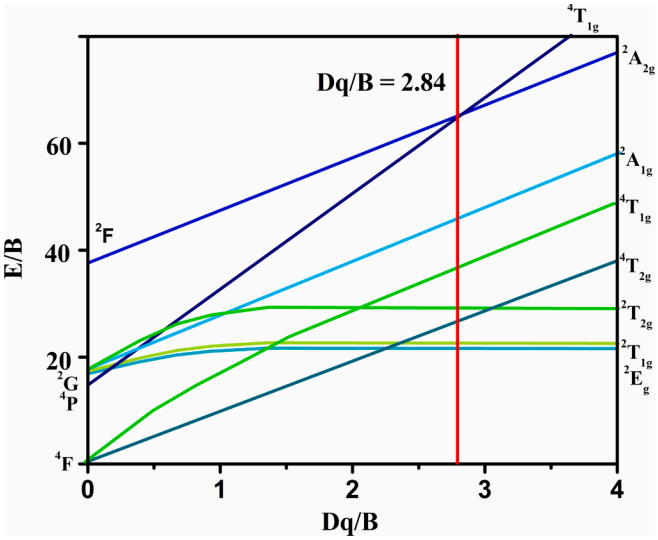

Fig. 5. Tanabe-Sugano energy-level diagram of Mn^{4+} in $GdAlO_3$ host.

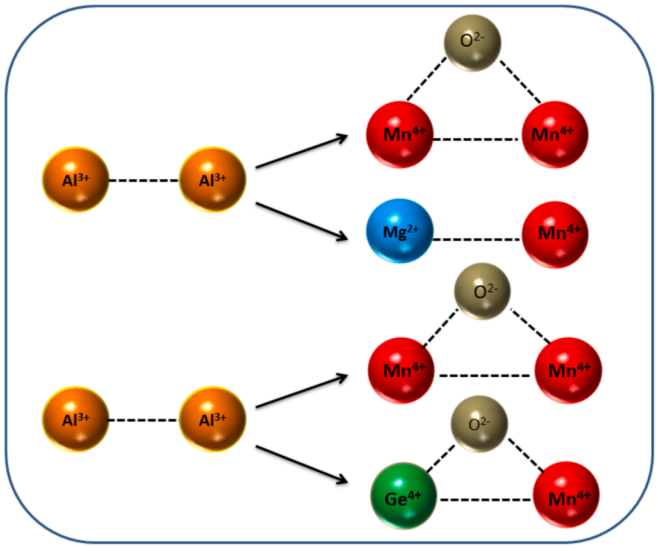

Fig. 6. Mechanism of improved Mn^{4+} luminescence via doping of Mg^{2+} and Ge^{4+}.

$$R_c \approx 2\left[\frac{3V}{4\pi X_C N}\right]^{\frac{1}{3}} \quad (3)$$

where V represents the volume of unit cell, N is the number of available occupations for the dopant in the unit cell, X_c stands for the critical concentration for Mn^{4+}. As for $GdAlO_3$ host, V = 207.41 $Å^3$, N = 4 and X_c = 0.5%. Therefore, R_c can be calculated by equation (3) and the value for $GdAlO_3$:xMn^{4+} is obtained to be 27.05 Å. The value is far beyond 5 Å, illustrating that the exchange interaction mechanism is unreasonable for the energy transfer among Mn^{4+} [31]. And we can utilize the following equation to confirm the type of interaction [32,33].

$$I/x = K\left[1+\beta(x)^{\theta/3}\right]^{-1} \quad (4)$$

where I is the PL intensity, x represents the activator concentration over the critical concentration, K and β stand for the constants. And θ = 6, 8, 10 denote the dipole-dipole (d-d), dipole-quadrupole (d-q), and quadrupole-quadrupole (q-q) interaction, respectively. Fig. 3(b) shows the relationship between lg (I/x) versus lg(x), which can be fitted by a straight line and slope is −1.73 (-θ/3). The value of θ is 5.19 closer to 6, which manifests that dipole-dipole interaction dominates for the emission quenching of Mn^{4+} ions in $GdAlO_3$:Mn^{4+} phosphors.

At the same time, we also investigated the luminescence behaviors of Mn^{4+} via different impurity doping. We doped three ions with same concentration to the $GdAlO_3$:0.5%Mn^{4+} samples. Fig. 4(a) shows the XRD patterns of different ions co-doped $GdAlO_3$:0.5%Mn^{4+}, which suggests the samples with different ions doping remain to be pure $GdAlO_3$ phase. Fig. 4(b) depicts the effects of Li^+, Mg^{2+}, Ge^{4+} on the emission intensities of $GdAlO_3$:Mn^{4+}. Mg^{2+} and Ge^{4+} are capable of improving the luminescence of $GdAlO_3$:Mn^{4+} phosphors, while Li^+ does not have obvious influence.

Generally, Mn^{4+} luminescence is prone to the crystal field strength and site symmetry of host, since the 3 d^3 electronic configuration of Mn^{4+} is the outer shell [34]. This can be depicted using the Tanabe-Sugano diagram, as demonstrated in Fig. 5 [12]. Generally, the electrons in $^4A_{2g}$ ground state transfer to the $^4T_{1g}$, $^2T_{2g}$ and $^4T_{2g}$ excited state under the excitation of 467 nm. The local crystal strength Dq can be obtained by the following equations [35,36].

$$Dq = E\ (^4A_{2g} \rightarrow {}^4T_{2g})/10 \quad (5)$$

On the basis of the formula and spectra, we can calculate the Dq = 2057.6 cm^{-1} (the wavenumber of $^4A_{2g} \rightarrow {}^4T_{2g}$ is 20576 cm^{-1}). In the Tanabe-Sugano diagram, the Racah parameter B is a critical parameter which can be expressed:

$$\frac{Dq}{B} = \frac{15(x-8)}{x^2-10x} \quad (6)$$

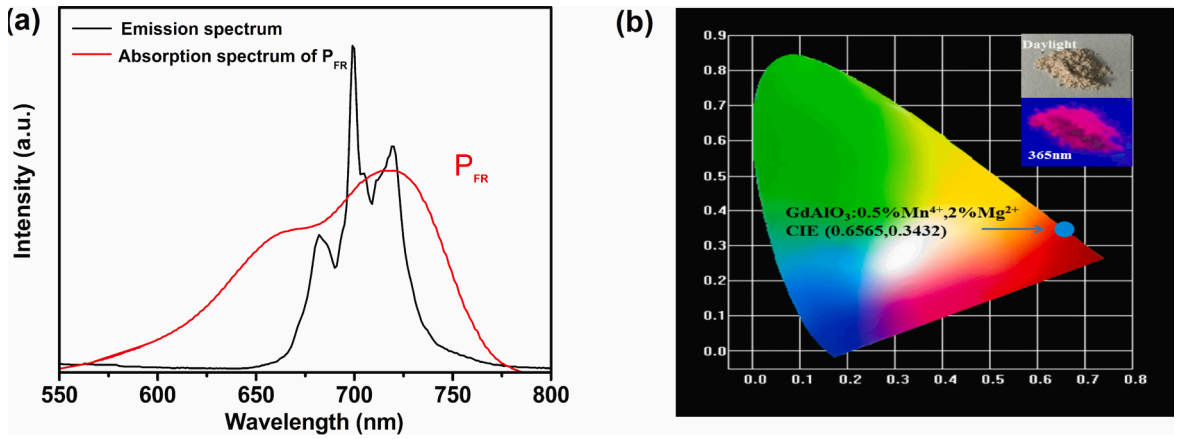

Fig. 7. (a) The PL spectrum of GAL: 0.5%Mn^{4+}, 2%Mg^{2+} under the excitation of 467 nm and the absorption spectrum of the phytochrome (P_{FR}); (b) The CIE chromaticity coordinate of GAL: 0.5%Mn^{4+}, 2%Mg^{2+}. Insets display the picture under daylight and a 365 nm UV lamp.

where the x can be calculated by the following expression:

$$x = \frac{E\left({}^4A_{2g} \rightarrow {}^4T_{1g}\right) - E\left({}^4A_{2g} \rightarrow {}^4T_{2g}\right)}{Dq} \quad (7)$$

Another Racah parameter C can be evaluated from the expression:

$$\frac{E\left({}^2E_g \rightarrow {}^4A_{2g}\right)}{B} = \frac{3.05C}{B} + 7.9 - \frac{1.8B}{Dq} \quad (8)$$

where E ($^4A_{2g}\rightarrow{}^4T_{1g}$), E ($^4A_{2g}\rightarrow{}^4T_{2g}$) and E ($^2E_g\rightarrow{}^4A_{2g}$) were 28011 cm^{-1}, 20576 cm^{-1} and 14326 cm^{-1} from the excitation spectra, respectively. Therefore, according to formula (5)-(8), the Dq/B, Racah parameter B and C were obtained to be 2.84, 721.9, 2975 cm^{-1}, respectively. The crystal field is seen as "strong" because the Dq/B overtops the value of 2.2, which is consistent with preliminary judgment from the emission spectrum [37].

It is noteworthy that Mg^{2+} ions are found to improve the luminescence of the $GdAlO_3$: Mn^{4+} most efficiently. Fig. 6 may explain the reason for the luminescence behavior. Mg^{2+} ions tend to substitute both Al^{3+} and Gd^{3+} sites, because the radius of Mg^{2+}(r = 0.72 Å, CN = 6) is the middle between the Al^{3+}(r = 0.53 Å, CN = 6) and Gd^{3+}(r = 0.938 Å, CN = 6). As a result of the different charge between Mn^{4+} and Al^{3+}, the charge compensation is required. On the one hand, Mg^{2+}-Mg^{2+} pairs substitute Gd^{3+}-Gd^{3+} pairs to compensate the charge. On the other hand, Mn^{4+}-Mg^{2+} pairs can also occupy Al^{3+}-Al^{3+}pairs in the absence of charge compensation. However, the existence of Mn^{4+}-Mg^{2+} pairs inhibited the energy migration among Mn^{4+} effectively [38]. As for Ge^{4+} co-doped $GdAlO_3$:Mn^{4+}samples, the ionic radius of Ge^{4+} (r = 0.54 Å, CN = 6) approaches to the ionic radius of Al^{3+}(r = 0.53 Å, CN = 6). Thus, Mn^{4+}-O^{2-}-Mn^{4+} can transfer Ge^{4+}-O^{2-}-Mn^{4+} and Ge^{4+} ions will interrupt the energy immigration among Mn^{4+} ions [39]. When Li^+ co-doped $GdAlO_3$:Mn^{4+} sample, the ionic radius of Li^+ (r = 0.92 Å, CN = 6) is closer to the ionic radius of Gd^{3+} (r = 0.938 Å, CN = 6). Hence, Li^+ ions have no ability to keep charge neutralization of the phosphors. So, we cannot find that co-doping Li^+ has any influence on Mn^{4+} luminescence.

3.3. Application of $GdAlO_3$:Mn^{4+} in plant-growth LEDs

Fig. 7(a) displays the emission spectrum of GAL: 0.5% Mn^{4+}, 2% Mg^{2+} phosphors and the absorption spectrum of phytochrome P_{FR}. There is a tremendous overlap between the absorption spectrum of phytochrome P_{FR} and the emission spectrum of GAL: 0.5%Mn^{4+}, 2% Mg^{2+}, which suggests that present phosphor has an expansive outlook for application in plant cultivation. In addition, GAL: 0.5%Mn^{4+}, 2%

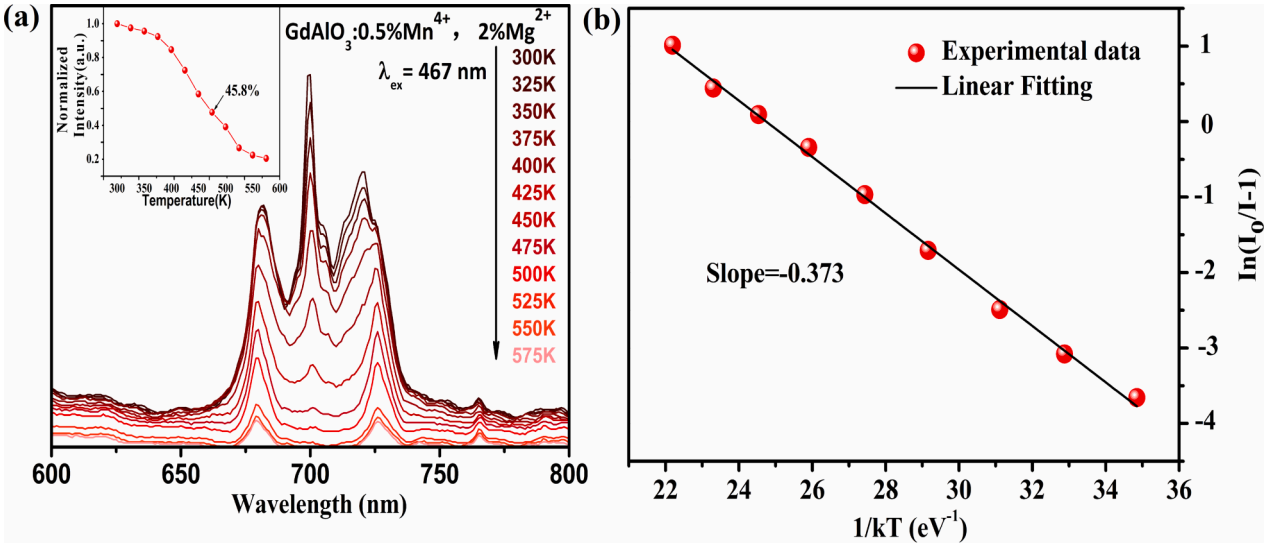

Fig. 8. (a) The temperature dependence of PL intensity of GAL: 0.5%Mn^{4+}, 2%Mg^{2+} under the excitation of 467 nm. Inset shows the normalized intensity of the PL intensity as a function of the temperature; (b) The dependence of ln (I/I_0-1) on 1/kT.

Table 1
The thermal activation energy of different phosphors.

Phosphors	Thermal activation energy	Ref.
$GdAlO_3:Mn^{4+}$	0.373eV	This work
$Ca_2LaTaO_6:Mn^{4+}$	0.320eV	[46]
$Li_5La_3Ta_2O_{12}:Mn^{4+}$	0.311eV	[47]
$Li_3Mg_2NbO_6:Mn^{4+}$	0.318eV	[48]
$Sr_2Si_5N_8:Eu^{2+}$	0.190eV	[49]
$Ca_2GdSbO_6:Mn^{4+}$	0.368eV	[50]
$Ba_2YNbO_6:Mn^{4+}$	0.315eV	[51]

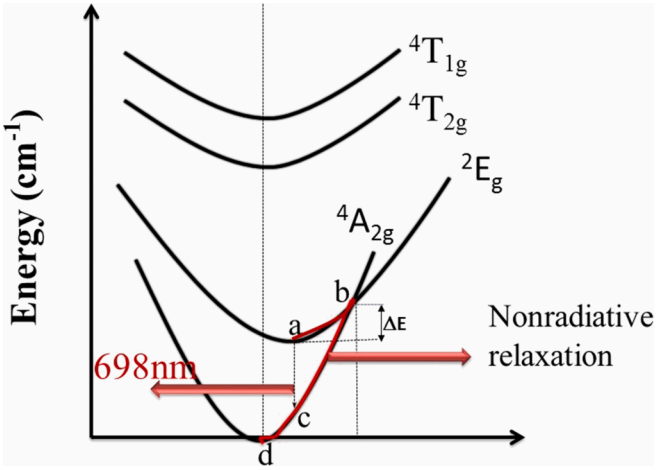

Fig. 9. Configurational coordinate diagram for Mn^{4+} ions in $GdAlO_3$.

Mg^{2+} is demonstrated with a quantum yield of 24% upon a 467 nm excitation, which is higher than some previous reported Mn^{4+} doped phosphors, such as $SrLaScO_4$: Mn^{4+}(PLQY = 12.2%), $Ca_{14}Al_{10}Zn_6O_{35}$: Mn^{4+}(PLQY = 19.4%) [40,41].

Fig. 7(b) illustrates the CIE chromaticity coordinates of GAL: 0.5% Mn^{4+}, 2%Mg^{2+}. The CIE chromaticity coordinates (0.6565, 0.3432) were obtained by the emission spectra of samples. In addition, we also calculated the color purity of phosphor according to the following formula [42].

$$\text{Color purity} = \sqrt{\frac{(x_s - x_i)^2 + (y_s - y_i)^2}{(x_d - x_i)^2 + (y_d - y_i)^2}} \quad (9)$$

Herein, (x_s, y_s) is the CIE chromaticity coordinates of the phosphors; (x_d, y_d) represents the CIE chromaticity coordinates of the dominant wavelength, which can be obtained by various of ways. (x_i, y_i) refers to the illuminant point of the 1931 CIE Standard Source C. The color purity of GAL: 0.5%Mn^{4+}, 2%Mg^{2+} phosphors is 99%, which implies that Mn^{4+} doped $GdAlO_3$ phosphors have high color purity.

As far as we know, the thermal stability capacity standard of phosphor is a crucial parameter in plant growth LEDs. Fig. 8(a) depicts temperature dependence of Mn^{4+} luminescence at different temperature. We utilize the normalized intensity of the PL intensity as a function of the temperature to obtain the temperature at which the emission intensity is half of that at 300 K. The study demonstrates the temperature at the emission intensity is half of that at 300 K is 469.5 K and the intensity of luminescence at 475 K is 45.8% of the luminescence intensity at room temperature (300 K), which shows $GdAlO_3$ doped with Mn^{4+} is a great material with good thermal stability.

The activation energy originating from thermal quenching process can be depicted by the next expression [43,44].

$$I = \frac{I_0}{1 + c\exp(-\Delta E/kT)} \quad (10)$$

I_0 and I are individually the luminescence intensity at the starting temperature and at temperature T. Where k is Boltzmann's constant, c is a constant and ΔE is thermal activation energy.

By transforming formula (10) to other forms:

$$I_0 / I - 1 = c\exp(-\Delta E / kT) \quad (11)$$

$$\ln(I_0 / I - 1) = \ln c - \Delta E/kT \quad (12)$$

Accordingly, the dependence of ln (I_0/I-1) on 1/kT with linear fitting is displayed in Fig. 8(b). The scope of straight line is −0.373, so ΔE is equal to 0.373 eV. Table 1 shows the thermal activation energy of some materials. The thermal activation energy ΔE of $GdAlO_3$ doped with Mn^{4+} is larger than other ΔE in many materials, which further suggests that Mn^{4+} doped $GdAlO_3$ phosphors have good thermal stability. Furthermore, the possible thermal quenching mechanism was put forward in Fig. 9. Generally speaking, the electrons of ground state $^4A_{2g}$ are excited to $^4T_{1g}$ or $^4T_{2g}$ under the excitation of 467 nm, then relax to the ^2E_g via non-radiative transition process [45]. Next, the electrons located in ^2E_g level would return the ground state $^4A_{2g}$ in two ways. One route is $^2E_g \rightarrow {}^4A_{2g}$ radiation process, which can emit 698 nm light at room temperature. The other route is that ^2E_g level absorbs enough energy to get the b point at the high temperature, then returns to d point through nonradiative relaxation process (a→b→d) and it can diminish the luminescence of samples [46].

4. Conclusion

In summary, far-red emitting GAL: xMn^{4+} materials were synthesized by a simple sol-gel method and the crystal structure, luminescence properties of phosphors were investigated systematically. Impressively, during the research, we found that impurity Mg^{2+} co-doping can boost the luminescence intensity of phosphors and we explained the possible reasons of improved luminescence in detail. The concentration quenching mechanism and the crystal-field parameters of the $GdAlO_3$ were investigated and analyzed. The high color purity, good thermal stability and the coinciding well with the absorption of phytochrome P_{FR} vigorously confirm that $GdAlO_3$:0.5%Mn^{4+}, 2%Mg^{2+} phosphor has a brilliant outlook in plant growth LED indoors.

Author contributions section

Xin Li: Conceptualization, Methodology, Software and Writing - Original Draft. **Wenhao Li:** Data curation, Software. **Mochen Jia:** Software. **Bofei Hou**: Supervision. **Huayao Wang**: Software, Validation. **Yang Xu**: software. **Mingxuan Zhang**: Supervision. **Zuoling Fu:** Writing- Reviewing, Writing - Review & Editing, Resources and Methodology.

Declaration of competing interest

No conflict of interest.

Acknowledgments

We thank the Project of the National Natural Science Foundation of China (No.11874182), Science and Technology Project of the 13th Five-Year Plan of Jilin Provincial Department of Education (No. JJKH20190179KJ) and Special funds for provincial industrial innovation in Jilin Province (No. 2018C043-4) for financial support.

References

[1] P.M. Pattison, J.Y. Tsao, G.C. Brainard, B. Bugbee, LEDs for photons, physiology and food, Nature 563 (2018) 493–500.
[2] N. Yeh, P. Yeh, N. Shih, O. Byadgi, T. Chih Cheng, Applications of light-emitting diodes in researches conducted in aquatic environment, Renew. Sustain. Energy Rev. 32 (2014) 611–618.

[3] N. Yeh, J.P. Chung, High-brightness LEDs—energy efficient lighting sources and their potential in indoor plant cultivation, Renew. Sustain. Energy Rev. 13 (2009) 2175–2180.

[4] O. Margit, V. Akvile, The effects of light-emitting diode lighting on greenhouse plant growth and quality, Agric. Food Sci. 22 (2013).

[5] L. Ma, D.J. Wang, Z.Y. Mao, Q.F. Lu, Z.H. Yuan, Investigation of Eu–Mn energy transfer in $A_3MgSi_2O_8$:Eu^{2+}, Mn^{2+} (A=Ca,Sr,Ba) for light-emitting diodes for plant cultivation, Appl. Phys. Lett. 93 (2008) 144101.

[6] H.G. Choi, B.Y. Moon, N.J. Kang, Effects of LED light on the production of strawberry during cultivation in a plastic greenhouse and in a growth chamber, Sci. Hortic. 189 (2015) 22–31.

[7] T. Ouzounis, E. Rosenqvist, C.O. Ottosen, Spectral effects of artificial light on plant physiology and secondary metabolism, Rev. 50 (2015) 1128.

[8] R. Hernández, C. Kubota, Physiological responses of cucumber seedlings under different blue and red photon flux ratios using LEDs, Environ. Exp. Bot. 121 (2016) 66–74.

[9] A. Tiwari, S.J. Dhoble, Tunable lanthanide/transition metal ion-doped novel phosphors for possible application in w-LEDs: a review, Luminescence 0 (2019) 1–30.

[10] K.H. Lin, M.Y. Huang, W.D. Huang, M.H. Hsu, Z.W. Yang, C.M. Yang, The effects of red, blue, and white light-emitting diodes on the growth, development, and edible quality of hydroponically grown lettuce (Lactuca sativa L. var. capitata), Sci. Hortic. 150 (2013) 86–91.

[11] Y. Wei, Z. Cheng, J. Lin, An overview on enhancing the stability of lead halide perovskite quantum dots and their applications in phosphor-converted LEDs, Chem. Soc. Rev. 48 (2019) 310–350.

[12] H. Chen, H. Lin, Q. Huang, F. Huang, J. Xu, B. Wang, Z. Lin, J. Zhou, Y. Wang, A novel double-perovskite Gd_2ZnTiO_6:Mn^{4+} red phosphor for UV-based w-LEDs: structure and luminescence properties, J. Mater. Chem. C 4 (2016) 2374–2381.

[13] E.H. Penilla, L.F. Devia, M.A. Duarte, C.L. Hardin, Y. Kodera, J.E. Garay, Gain in polycrystalline Nd-doped alumina: leveraging length scales to create a new class of high-energy, short pulse, tunable laser materials, Light Sci. Appl. 7 (2018) 33.

[14] J. Deng, H. Zhang, X. Zhang, Y. Zheng, J. Yuan, H. Liu, Y. Liu, B. Lei, J. Qiu, Ultrastable red-emitting phosphor-in-glass for superior high-power artificial plant growth LEDs, J. Mater. Chem. C 6 (2018) 1738–1745.

[15] G. Tamulaitis, P. Duchovskis, Z. Bliznikas, K. Breive, R. Ulinskaite, A. Brazaityte, A. Novičkovas, A. Žukauskas, High-power light-emitting diode based facility for plant cultivation, J. Phys. D Appl. Phys. 38 (2005) 3182–3187.

[16] J. Liang, L. Sun, B. Devakumar, S. Wang, Q. Sun, H. Guo, B. Li, X. Huang, Far-red-emitting double-perovskite $CaLaMgSbO_6$: Mn^{4+} phosphors with high photoluminescence efficiency and thermal stability for indoor plant cultivation LEDs, RSC Adv. 8 (2018) 31666–31672.

[17] F. Zhou, F. Qiu, C. Wang, S. Xin, M. Gao, Z. Li, G. Zhu, Synthesis and photoluminescence properties of double perovskite phosphor $Ba_6Y_2W_3O_{18}$: Mg^{2+}, Mn^{4+} for plant cultivation, ECS J. Solid State Sci. Technol. 8 (2019) R119–R126.

[18] Y. Wu, Y. Lv, K. Ruan, Z. Xie, A far-red emission $(Ca,Sr)_{14}Zn_6Ga_{10}O_{35}$:$Mn^{4+}$ phosphor for potential application in plant-growth LEDs, Dalton Trans. 47 (2018) 15574–15582.

[19] R. Venkatesh, N. Dhananjaya, M.K. Sateesh, J.P. Shabaaz Begum, S.R. Yashodha, H. Nagabhushana, C. Shivakumara, Effect of Li, Na, K cations on photoluminescence of $GdAlO_3$:Eu^{3+} nanophosphor and study of Li cation on its antimicrobial activity, J. Alloy. Comp. 732 (2018) 725–739.

[20] J.M. Liu, Y.Y. Liu, D.D. Zhang, G.-Z. Fang, S. Wang, Synthesis of $GdAlO_3$:Mn^{4+},Ge^{4+}@Au core–shell nanoprobes with plasmon-enhanced near-infrared persistent luminescence for in vivo trimodality bioimaging, ACS Appl. Mater. Interfaces 8 (2016) 29939–29949.

[21] B. Wang, H. Lin, F. Huang, J. Xu, H. Chen, Z. Lin, Y. Wang, Non-rare-earth $BaMgAl_{10-2x}O17$:xMn^{4+},xMg^{2+}: a narrow-band red phosphor for use as a high-power warm w-LED, Chem. Mater. 28 (2016) 3515–3524.

[22] Q. Sun, S. Wang, B. Devakumar, L. Sun, J. Liang, X. Huang, Y. Wu, $CaYAlO_4$:Mn^{4+}, Mg^{2+}: an efficient far-red-emitting phosphor for indoor plant growth LEDs, J. Alloy. Comp. 785 (2019) 1198–1205.

[23] Q. Zhou, L. Dolgov, A.M. Srivastava, L. Zhou, Z. Wang, J. Shi, M.D. Dramićanin, M. G. Brik, M. Wu, Mn^{2+} and Mn^{4+} red phosphors: synthesis, luminescence and applications in WLEDs. A review, J. Mater. Chem. C 6 (2018) 2652–2671.

[24] R. Cao, J. Zhang, W. Wang, Z. Hu, T. Chen, Y. Ye, X. Yu, Preparation and photoluminescence characteristics of $Li_2Mg_3SnO_6$:Mn^{4+} deep red phosphor, Mater. Res. Bull. 87 (2017) 109–113.

[25] R. Cao, Y. Ye, Q. Peng, G. Zheng, H. Ao, J. Fu, Y. Guo, B. Guo, Synthesis and luminescence characteristics of novel red-emitting $Ba_2TiGe_2O_8$:Mn^{4+} phosphor, Dyes Pigments 146 (2017) 14–19.

[26] T. Fujii, K. Kodaira, O. Kawauchi, N. Tanaka, H. Yamashita, M. Anpo, Photochromic behavior in the fluorescence spectra of 9-Anthrol encapsulated in Si−Al glasses prepared by the Sol−Gel method, J. Phys. Chem. B 101 (1997) 10631–10637.

[27] J. Park, G. Kim, Y.J. Kim, Luminescent properties of $CaAl_4O_7$ powders doped with Mn^{4+} ions, Ceram. Int. 39 (2013) S623–S626.

[28] D.L. Dexter, J.H. Schulman, Theory of concentration quenching in inorganic phosphors, J. Chem. Phys. 22 (1954) 1063–1070.

[29] M.N. Bailey, G.K. Schweitzer, The mechanochemical and solution combustion syntheses of cerium-doped lutetium oxyorthosilicate powder, J. Alloy. Comp. 734 (2018) 258–265.

[30] S.K. Hussain, T.T.H. Giang, J.S. Yu, UV excitation band induced novel $Na_3Gd(VO_4)_2$:RE^{3+} (RE^{3+} = Eu^{3+} or Dy^{3+} or Sm^{3+}) double vanadate phosphors for solid-state lightning applications, J. Alloy. Comp. 739 (2018) 218–226.

[31] L. Sun, B. Devakumar, J. Liang, S. Wang, Q. Sun, X. Huang, Simultaneously enhanced far-red luminescence and thermal stability in $Ca_3Al_4ZnO_{10}$:Mn^{4+} phosphor via Mg^{2+} doping for plant growth lighting, J. Alloy. Comp. 785 (2019) 312–319.

[32] Y. Zhou, E. Song, T. Deng, Y. Wang, Z. Xia, Q. Zhang, Surface passivation toward highly stable Mn^{4+}-activated red-emitting fluoride phosphors and enhanced photostability for white LEDs, Advanced Materials Interfaces 6 (2019) 1802006.

[33] Y. Jin, Y. Hu, H. Wu, H. Duan, L. Chen, Y. Fu, G. Ju, Z. Mu, M. He, A deep red phosphor Li_2MgTiO_4:Mn^{4+} exhibiting abnormal emission: potential application as color converter for warm w-LEDs, Chem. Eng. J. 288 (2016) 596–607.

[34] S. Liang, G. Li, P. Dang, Y. Wei, H. Lian, J. Lin, Cation substitution induced adjustment on lattice structure and photoluminescence properties of $Mg_{14}Ge_5O_{24}$:Mn^{4+}: optimized emission for w-LED and thermometry applications, Adv. Opt. Mater. 7 (2019) 1900093.

[35] D. Chen, W. Xu, S. Yuan, X. Li, J. Zhong, Ln^{3+}-Sensitized Mn^{4+} near-infrared upconverting luminescence and dual-modal temperature sensing, J. Mater. Chem. C 5 (2017) 9619–9628.

[36] H. Lin, T. Hu, Q. Huang, Y. Cheng, B. Wang, J. Xu, J. Wang, Y. Wang, Non-rare-earth K_2XF_7:Mn^{4+} (X = Ta, Nb): a highly-efficient narrow-band red phosphor enabling the application in wide-color-gamut LCD, Laser Photonics Rev. 11 (2017) 1700148.

[37] T.P.P. Hall, W. Hayes, R.W.H. Stevenson, J. Wilkens, Investigation of the bonding of iron-group ions in fluoride crystals. I, J. Chem. Phys. 38 (1963) 1977–1984.

[38] M.G. Brik, Y.X. Pan, G.K. Liu, Spectroscopic and crystal field analysis of absorption and photoluminescence properties of red phosphor $CaAl_{12}O_{19}$:Mn^{4+} modified by MgO, J. Alloy. Comp. 509 (2011) 1452–1456.

[39] W. Shu, L. Jiang, S. Xiao, X. Yang, J.W. Ding, GeO_2 dopant induced enhancement of red emission in $CaAl_{12}O_{19}$:Mn^{4+} phosphor, Mater. Sci. Eng., B 177 (2012) 274–277.

[40] U.B. Humayoun, S.N. Tiruneh, D.-H. Yoon, On the crystal structure and luminescence characteristics of a novel deep red emitting $SrLaScO_4$:Mn^{4+}, Dyes Pigments 152 (2018) 127–130.

[41] J.Y. Park, J.S. Joo, H.K. Yang, M. Kwak, Deep red-emitting $Ca_{14}Al_{10}Zn_6O_{35}$:Mn^{4+} phosphors for WLED applications, J. Alloy. Comp. 714 (2017) 390–396.

[42] M. Zhu, Y. Pan, M. Wu, H. Lian, J. Lin, Synthesis and improved photoluminescence of a novel red phosphor $LiSrGaF_6$:Mn^{4+} for applications in warm WLEDs, Dalton Trans. 47 (2018) 12944–12950.

[43] Q. Wang, J. Liao, L. Kong, B. Qiu, J. Li, H. Huang, H.-r. Wen, Luminescence properties of a non-rare-earth doped oxyfluoride $LiAl_4O_6F$:Mn^{4+} red phosphor for solid-state lighting, J. Alloy. Comp. 772 (2019) 499–506.

[44] R.J. Xie, N. Hirosaki, N. Kimura, K. Sakuma, M. Mitomo, 2-phosphor-converted white light-emitting diodes using oxynitride/nitride phosphors, Appl. Phys. Lett. 90 (2007) 191101.

[45] Z. Lu, Y. Meng, L. Wen, M. Huang, L. Zhou, L. Liao, D. He, Double perovskite Ba_2LaNbO_6:Mn^{4+},Yb^{3+} phosphors: potential application to plant-cultivation LEDs, Dyes Pigments 160 (2019) 395–402.

[46] R. Cao, T. Chen, Y. Ren, T. Chen, H. Ao, W. Li, G. Zheng, Synthesis and photoluminescence properties of Ca_2LaTaO_6:Mn^{4+} phosphor for plant growth LEDs, J. Alloy. Comp. 780 (2019) 749–755.

[47] R. Cao, X. Lv, Y. Ran, L. Xu, T. Chen, S. Guo, H. Ao, X. Yu, Rare-earth-free $Li_5La_3Ta_2O_{12}$:Mn^{4+} deep-red-emitting phosphor: synthesis and photoluminescence properties, J. Am. Ceram. Soc. 102 (2019) 5910–5918.

[48] X. Wang, X. Zhou, Y. Cao, Q. Wei, Z. Zhao, Y. Wang, Insight into a novel rare-earth-free red-emitting phosphor $Li_3Mg_2NbO_6$:Mn^{4+}: structure and luminescence properties, J. Am. Ceram. Soc. 102 (2019) 6724–6731.

[49] S.E. Brinkley, N. Pfaff, K.A. Denault, Z.J. Zhang, Robust thermal performance of $Sr_2Si_5N_8$:Eu^{2+}: an efficient red emitting phosphor for light emitting diode based white lighting, Appl. Phys. Lett. 99 (2011) 241106.

[50] J. Liang, B. Devakumar, L. Sun, Q. Sun, S. Wang, X. Huang, Novel Mn^{4+} doped Ca_2GdSbO_6 red–emitting phosphor: a potential color converter for light-emitting diodes, J. Am. Ceram. Soc. 102 (2019) 4730–4736.

[51] A. Fu, Q. Pang, H. Yang, L. Zhou, Ba_2YNbO_6:Mn^{4+}-based red phosphor for warm white light-emitting diodes (WLEDs): photoluminescent and thermal characteristics, Opt. Mater. 70 (2017) 144–152.